Optimization of Mono- and Bi-Articular Parallel Elastic Elements for a Robotic Arm Performing a Pick-and-Place Task

Maxime Marchal, Raphaël Furnémont, Bram Vanderborght, *Senior Member, IEEE*, Ghilès Mostafaoui, and Tom Verstraten, *Member, IEEE*

***Abstract*—Actuation concepts such as Series Elastic Actuation (SEA), Parallel Elastic Actuation (PEA), and Biarticular Actuation (BA), which introduce elastic elements into the structure, have the potential to reduce the electrical energy consumption of a robot. This letter presents an optimization of the arrangement of springs for a 3 degrees of freedom robotic arm, with the aim of decreasing the electrical energy consumption for a given pick-and-place task. Through simulations and experimental validation, we show that the optimal configuration in terms of electrical energy consumption and complexity consists of rigid actuation on joint 1 and PEAs on joints 2 and 3. With this configuration, root mean square (RMS) and peak load torques for a specific pick-and-place task can be reduced respectively by up to 43% and 44% for joint 2, and by 15% and 21% for joint 3 compared to the configuration without springs.**

***Index Terms*—Actuation and Joint Mechanisms, Compliant Joints and Mechanisms, Robotics and Automation in Construction, Mechanism Design, Product Design.**

I. Introduction

With the cost of electricity on the rise, energy-efficient design of robots is receiving increased attention. Introducing elastic elements in the joints and robot structure, can help reducing energy consumption [1]. Indeed, elastic elements can store and release energy without going through the actuator and lose energy due to motor and transmission losses. The two most known methods to reduce consumption are Series Elastic Actuation (SEA) and Parallel Elastic Actuation (PEA). The first concept relies on an elastic element, typically a spring, in series between the actuator and the load [2]. SEAs allow to reduce the peak power [3], improve efficiency by storing and releasing energy [4], and decouple the reflected inertia of the actuator from the inertia of the load [5]. For example, [6] has demonstrated the advantages of implementing SEA in a prosthetic leg in terms of energy-efficiency. The other common arrangement (i.e., PEA) consists of placing the spring in parallel with the actuator with respect to the load [7]. It allows to decrease the actuator's torque requirements leading to an increase of the energy efficiency [8] and increase the system's stability [9]. More specifically, [10] has proven the benefits of adding parallel springs in a robotic arm in terms of energy consumption and torque requirements.

Another concept, based on the musculature of humans and animals, is Biarticular Actuation (BA). As its name suggests, BA means simultaneous actuation of two joints of the robot by only one actuator [11] or a passive component like a spring [12]. BA offers the possibility to transfer mechanical power between joints [13], in particular from proximal towards distal joints [14], leading to an improvement in energy efficiency [15]. Such actuation also produces a maximum end-effector force in a more homogeneously distributed way [16], eases the control [17], and simplifies the dynamic equations [18]. For example, [19] has shown that implementing biarticular mechanisms in robotic manipulators can help to increase their energy efficiency.

As PEA and BA are not mutually exclusive, it is also possible to combine both in an attempt to simultaneously exploit the benefits of each. [20] has already combined both in a robotic leg, but only the placement of the actuators and the best actuation scheme have been optimized, and not the springs' characteristics (stiffness, equilibrium angle, etc.). [21] and [22] have optimized the springs' characteristics for respectively a robotic leg and a robotic arm, but not in terms of actuator torque requirements. To the best of the authors' knowledge, an optimal configuration of PEA and BA in terms of actuator torque requirements in a single robotic arm has only been investigated in [17]. Nevertheless, the type of BA considered in our paper is not the same, which makes our contribution novel. Indeed, in the work of [17], BA refers to the simultaneous actuation of two joints of the robot by only one actuator, while in our work, BA is considered as the simultaneous actuation of two joints of the robot by a single spring.

In this work, we present a methodology to find the most energy-optimal configuration of PEA and BA for a 3 degrees

Manuscript received 1 March 2023; accepted 18 June 2023. Date of publication 28 June 2023; date of current version 11 July 2023. This letter was recommended for publication by Associate Editor X. LI and Editor C. Gosselin upon evaluation of the reviewers' comments. This work was supported in part by EUTOPIA Co-Tutelle, and in part by the FWO Projects under Grants S001821N and 1505820N. *(Corresponding author: Maxime Marchal.)*

Maxime Marchal, Raphaël Furnémont, and Tom Verstraten are with Robotics & Multibody Mechanics Research Group, Faculty of Mechanical Engineering, Vrije Universiteit Brussel, 1050 Elsene, Belgium, and also with Flanders Make, 3290 Lommel, Belgium (e-mail: maxime.geoffroy.y.marchal@vub.be; raphael.furnemont@vub.be; tom.verstraten@vub.ac.be).

Bram Vanderborght is with Robotics & Multibody Mechanics Research Group, Faculty of Mechanical Engineering, Vrije Universiteit Brussel, 1050 Elsene, Belgium, and also with IMEC, 3001 Leuven, Belgium (e-mail: bram.vanderborght@vub.ac.be).

Ghilès Mostafaoui is with ETIS, CY Cergy Paris Université, 95000 Cergy-Pontoise, France (e-mail: ghiles.mostafaoui@ensea.fr).

This letter has supplementary downloadable material available at https://doi.org/10.1109/LRA.2023.3290518, provided by the authors.

Digital Object Identifier 10.1109/LRA.2023.3290518

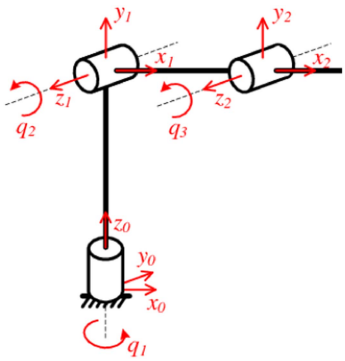

Fig. 1. Articulated robotic arm of RRR type. The joint angles were defined using the Denavit–Hartenberg convention.

TABLE I
MECHANICAL PARAMETERS OF THE ROBOTIC ARM

	Link 1	Link 2	Link 3
$m\ (kg)$	4.480	4.045	2.181
$l\ (m)$	0.07	0.3	0.3
$l_c\ (m)$	$5.08e-2$	$8.06e-2$	$1.08e-1$
$I_{xx}\ (kg\ m^2)$	$6.292e-2$	$1.440e-2$	$4.90e-3$
$I_{xy}\ (kg\ m^2)$	0	$4.9e-4$	0
$I_{xz}\ (kg\ m^2)$	$6.49e-3$	$9.67e-3$	$2.4e-4$
$I_{yy}\ (kg\ m^2)$	$3.266e-2$	$6.831e-2$	$6.839e-2$
$I_{yz}\ (kg\ m^2)$	0	0	0
$I_{zz}\ (kg\ m^2)$	$6.292e-2$	$5.738e-2$	$6.460e-2$
	Joint 1	Joint 2	Joint 3
$\dot{q}_{max}\ (^\circ/s)$	90	90	90
$\ddot{q}_{max}\ (^\circ/s^2)$	180	180	180

of freedom robotic arm (RRR type), actuated by servo actuators, performing a pick-and-place task. More specifically, it consists of finding the optimal arrangement of springs and their characteristics to achieve the lowest possible root mean square (RMS) and peak load torque for a given pick-and-place task of the robotic arm. In addition to the simulations, a prototype has been built to validate them.

The paper is organized as follows: Section II describes the model and the task. Section III explains the influence of the elastic elements on the equations of motion of the robotic arm, the actuator electrical energy consumption, and the optimization procedure. Section IV describes the prototype built to validate the results obtained with the simulations. Section V shows the results regarding the optimal configuration in terms of load torque. Finally, Section VI concludes the results and discusses the limitations and future work.

II. MODEL AND TASK DESCRIPTION

A. Model

The type of robotic arm treated in this letter is of RRR type (Fig. 1). In this robotic arm, there are three electrical servo actuators, where each is controlling a single joint. All the mechanical parameters are given in Table I. They have been found by using CAD software (Inventor) and validated experimentally, where stress analysis has been performed to ensure that the prototype built (see Section IV) with these parameters can handle a payload of 5 kg. Furthermore, limits of maximal angular velocities have been chosen very close to the ones of the Kuka LBR iiwa 7 R800 to ensure safety, and maximal accelerations have been imposed to ensure smooth operation of the actuators. The equations of motion of the robot are given by [23]:

$$M(q)\ddot{q} + C(q,\dot{q})\dot{q} + G(q) = \tau_l \tag{1}$$

where $M(q)$ is the mass matrix (also called inertia matrix), q are the joint displacements, $C(q,\dot{q})$ is the matrix of Coriolis and centrifugal forces, $G(q)$ is the gravitational torque vector, and τ_l is the load torque vector (also called the input torque seen by the actuator). Note that $M(q)$, $C(q,\dot{q})$, and $G(q)$ can be derived from Table I using Lagrangian mechanics.

B. Task

In the manufacturing industry, robotic manipulators are commonly employed to move objects from one position to another. They often work in chains and repeatedly execute pick-and-place tasks, where speed and consistency are important features. To increase the industrial relevance of our results, we consider a pick-and-place task in our work as well. Indeed, pick-and-place tasks cover a lot of applications (palletizing, bin picking, etc.) for which there is a payload close to the maximum load that the robot can handle, and where elastic actuation can help to decrease the actuators' torque requirements. The pick-and-place task considered in this work is composed of 3 phases: 1) The robotic arm moves from its initial position to a known release position by carrying a payload of 5 kg (called go phase), 2) The robotic arm releases the payload (called releasing phase), and 3) The robotic arm comes back to the initial position without the payload (called return phase). To ensure continuity in the equations and a coherent continuous definition of the predefined end-effector spatiotemporal trajectory, a linear decrease of the payload's mass instead of an abrupt one is assumed for the releasing phase. Nevertheless, this phase is not considered for the spring parameters optimization and the experiments on the prototype for two main reasons. First, this phase is much shorter than the go and return phases in industrial applications where robotic manipulators perform pick-and-place tasks. Therefore, it has almost no impact on the optimization. Second, with the current hardware, it is not possible to consider this phase during experiments on the prototype. Indeed, there is no gripper installed and no degree of freedom at the end-effector of the prototype that allows releasing the payload properly during experiments. As a result, only the go and return phases are considered in the optimization and experiments. The initial/final position chosen is $x_0 = x_f = 0.15\,\mathrm{m}, \mathrm{y}_0 = \mathrm{y}_\mathrm{f} = 0.15\,\mathrm{m}, \mathrm{z}_0 = 0.07\,\mathrm{m}$ and the release one is $x_r = 0.4\,\mathrm{m}, \mathrm{y}_\mathrm{r} = -0.4\,\mathrm{m}, \mathrm{z}_\mathrm{r} = 0.07\,\mathrm{m}$ as displayed in Fig. 2 where only the $x-z$ view is shown for clarity purpose. Note that the initial and release positions have been chosen so that the three joints move significantly during the task, namely joint 1 between -45° and 45°, joint 2 between 19.5° and 69.3°, and joint 3 between -138.6° and -38.9°. It is also important to mention that for such a robotic arm, there exist two configurations of joints for which a single end-effector position is possible, namely elbow-up and elbow-down configurations.

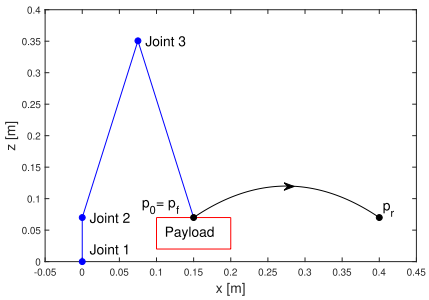

(a) Go phase

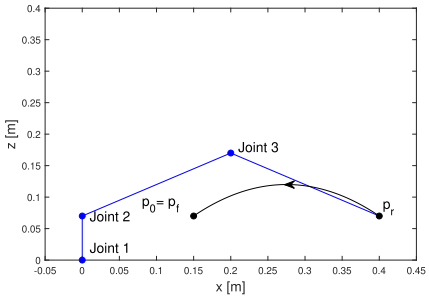

(b) Return phase

Fig. 2. Pick-and-place task. p_0 stands for the initial position, p_f stands for the final position, and p_r is the release position.

Nevertheless, only the elbow-up configuration is considered here because it induces fewer collisions than the elbow-down configuration. As a result, one end-effector position corresponds to a single angular position of the joints.

In this letter, only one fixed trajectory is considered. This trajectory is defined by a polynomial of 5^{th}-order where its initial and final angular positions are given, where its initial and final angular velocities and accelerations are set to zero, and where its initial and final times are predetermined. Therefore, there exists only one trajectory that respects these constraints, and which can be expressed by:

$$q_i(t) = q_i(t_0) + \left(\frac{q_i(t_f) - q_i(t_0)}{t_f^3}\right)\left(\frac{6}{t_f^2}t^5 - \frac{15}{t_f}t^4 + 10t^3\right) \tag{2}$$

where t is the time vector (which is also imposed), $i = 1, 2, 3$ represent the 3 joints, and the indices 0 and f are respectively for initial and final times. The trajectory is reversed for the return phase. Note that the angular velocities and acceleration can be derived from (2) by differentiation with respect to the time. Due to the angular velocities and accelerations limits imposed to ensure safety, the durations chosen for the go phase, releasing phase, and return phase are fixed and are respectively 3 s, 1 s, 3 s to give equal weight to the go and return phases for the optimization.

Before describing more in detail the different types of elastic actuation presented in Section I, it is important to note that the simulations have shown that implementing a SEA for the task considered is not load torque efficient for any joints. For joints 2 and 3 this can be easily explained by the fact that the gravitational

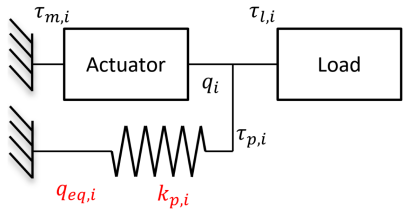

Fig. 3. Parallel Elastic Actuation (PEA). τ_m is the motor torque and $i = 2, 3$ represent joints 2 and 3. A positive value of $q_i - q_{eq,i}$ corresponds to the compression of the corresponding parallel spring, and therefore to the production of a torque.

torques acting on those joints are by far higher than the torques due to the dynamics, namely the inertia, Coriolis, and centrifugal torques. In joint 1, where gravity has no influence, a series spring does not improve the system's energy efficiency because the trajectory is prescribed by a 5^{th}-order polynomial, i.e. the joint trajectory is not optimized, preventing natural dynamics from being exploited. That is why SEA will not be investigated anymore in this letter. Moreover, the electrical energy consumption of the actuator placed on joint 1 is very low compared to the ones of the whole system. Therefore, only joints 2 and 3 will be studied ($\tau_{p,1} = 0$ and $\tau_{b,1} = 0$).

III. Optimization Procedure of the Parallel and Biarticular Elements

A. Parallel Elastic Actuation (PEA)

PEAs rely on a spring placed in parallel with the actuator with respect to the load (Fig. 3). It is considered as a monoarticular elastic actuation since it produces a torque only on the joint on which the parallel spring is placed.

When a PEA is considered, (1) becomes:

$$M(q)\ddot{q} + C(q, \dot{q})\dot{q} + G(q) = \tau_l + \tau_p \tag{3}$$

where τ_p is the torque produced by the PEAs present on each joint. Since only unidirectional spiral torsion springs are considered, τ_p is given by:

$$\tau_{p,i} = \begin{cases} -k_{p,i}(q_i - q_{eq,i}) & \text{if } q_i \geq q_{eq,i} \\ 0 & \text{else} \end{cases} \tag{4}$$

where $k_{p,i}$ is the spring stiffness of the parallel springs, $q_{eq,i}$ is the equilibrium angle of the corresponding springs, and $i = 2, 3$ represents joints 2 and 3. The torque produced by the unidirectional spiral torsion spring is null when $q_i < q_{eq,i}$ because the extremity of this spring is not in contact anymore with the shaft on which it is supposed to rest in order to produce torque. Therefore, the spring is not deflected, meaning that it does not produce any torque. One can also see that optimizing PEA corresponds in reality to optimize two parameters, namely the stiffness $k_{p,i}$ and the equilibrium angle of the spring $q_{eq,i}$. Note that if the orientation of the unidirectional spiral torsion spring is inverted, meaning that it starts to compress when $q_i \leq q_{eq,i}$, the condition of (4) becomes $q_i \leq q_{eq,i}$. As a result, depending on the orientation of the spring, the direction of the torque that the parallel spring of the PEA unit can produce is

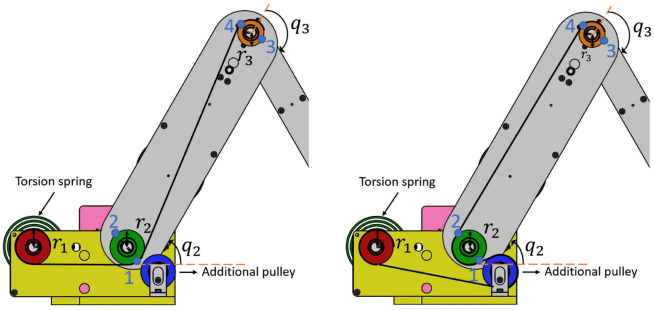

(a) Arrangement A (b) Arrangement D

Fig. 4. Biarticular Parallel Elastic Actuation (BPEA). Arrangement B can be obtained by connecting points 2 and 3 in (b) and Arrangement C by connecting points 1 and 3 in (a).

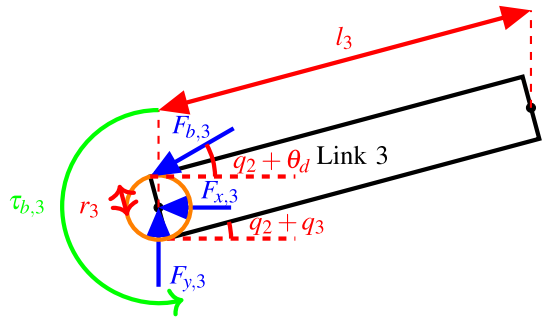

Fig. 5. Free body diagram of Link 3 with BPEA of Arrangement D. $F_{x,3}$ is the horizontal reaction force on Joint 3, $F_{y,3}$ is the vertical reaction force on Joint 3, $F_{b,3}$ is the force of the BPEA on Joint 3, and θ_d is equal to $-\arcsin\frac{r_2-r_3}{l_2}$ for Arrangement D. Note that gravitational forces have been removed for clarity and that the values of $F_{b,3}$ and θ_d are dependent on the type of Arrangement. Values of $F_{b,3}$ are given in Table II.

not the same. That is why both cases are considered in the optimization.

B. Biarticular Parallel Elastic Actuation (BPEA)

Biarticular actuation refers to the simultaneous actuation of two joints by only one actuator or a passive component like a spring. In this letter, since there is already an actuator controlling each joint, no additional actuator will be considered as to not obtain a redundant robotic arm. Instead, a spring is placed with a biarticular connection. As such, we have created a PEA which spans not only one, but two joints, which we will refer to as "Biarticular Parallel Elastic Actuation" (BPEA). Nevertheless, there are different possibilities to produce a BPEA, among which two of them have been investigated: (1) Use of tension springs and (2) Use of spiral torsion springs. In the end, the second option has been chosen because its implementation is more practical. Indeed, spiral torsion springs produce a torque proportional to their deflection, which makes their implementation simple for a robot arm where all the joints are rotational. Therefore, BPEA in this letter is achieved through the use of a unidirectional spiral torsion spring, a LIROS D-Pro Dyneema cable, and 3 or 4 pulleys depending on the arrangement (Fig. 4).

First, the spring is connected to a shaft attached to link 1 (yellow part in Fig. 4) that can rotate freely thanks to bearings, and a red pulley is attached to this shaft. Then, one side of the Dyneema cable is attached to this red pulley, while the other is attached to a orange pulley connected to joint 3. This cable is also passing over a green pulley attached to joint 2 that can freely rotate, and over a blue additional pulley in some cases that can also freely rotate. Indeed, in this letter, four different arrangements of BPEA are examined, which leads to different torques produced at the corresponding joints. The first one, namely the one represented in Fig. 4(a), is when the Dyneema cable passes through Points 1 and 4 and is called Arrangement A. The second one is joining Points 2 and 3 and is called Arrangement B, while the third one is connecting Points 1 and 3 (Arrangement C). Finally, the last one is joining Points 2 and 4 and is called Arrangement D (Fig. 4(b)). Therefore, one can see that the blue additional pulley is only useful to obtain Arrangements B and D and is not used for Arrangements A and C. The torques produced by those

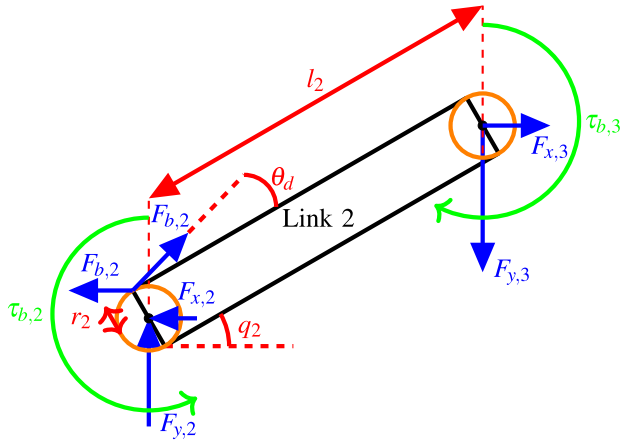

Fig. 6. Free body diagram of Link 2 with BPEA of Arrangement D. $F_{x,2}$ is the horizontal reaction force on Joint 2, $F_{y,2}$ is the vertical reaction force on Joint 2, and $F_{b,2}$ is the force of the BPEA on Joint 2. Note that gravitational forces have been removed for clarity and that the value of $F_{b,2}$ is the same as $F_{b,3}$. Values of $F_{b,2}$ are given in Table II.

arrangements are given in Table II and are found by solving the static equilibrium equations for links 2 and 3 as shown for Arrangement D in Figs. 5 and 6.

When optimizing a BPEA, there are five parameters to optimize, namely k, r_1, r_2, r_3, and q_0. r_1, r_2, and r_3 are respectively the radius of the pulleys placed on link 1, joint 2, and joint 3, k_b is the spring stiffness, and q_0 is the equilibrium angle of the spring. However, to simplify the optimization and respect available catalogue values while still finding a solution very close to the optimal solution, only four possibilities for r_2 and r_3 have been examined. Moreover, the same value has been selected for r_1 and r_2 to simplify the equations: since the torque produced by the BPEA is proportional to k_b but inversely proportional to r_1, the value of r_1 can be chosen arbitrarily when k_b is included as an optimization parameter.

With BPEA, (1) becomes:

$$M(q)\ddot{q} + C(q,\dot{q})\dot{q} + G(q) = \tau_l + \tau_b \tag{5}$$

TABLE II
TORQUES GENERATED BY THE 4 ARRANGEMENTS OF A BIARTICULAR PARALLEL ELASTIC ACTUATION ON JOINTS 2 AND 3

	$\tau_{b,2}$	$\tau_{b,3}$	Condition for $\tau_b \neq 0$	$F_{2,b} = F_{3,b}$
A	$-\frac{k_b}{r_1^2} r_2 (r_2 q_2 - r_3 q_3 + r_1 q_0)$	$\frac{k_b}{r_1^2} r_3 (r_2 q_2 - r_3 q_3 + r_1 q_0)$	$r_2 q_2 - r_3 q_3 + r_1 q_0 > 0$	$-\frac{k_b}{r_1^2} (r_2 q_2 - r_3 q_3 + r_1 q_0)$
B	$\frac{k_b}{r_1^2} r_2 (-r_2 q_2 + r_3 q_3 - r_1 q_0)$	$-\frac{k_b}{r_1^2} r_3 (-r_2 q_2 + r_3 q_3 - r_1 q_0)$	$-r_2 q_2 + r_3 q_3 - r_1 q_0 > 0$	$-\frac{k_b}{r_1^2} (-r_2 q_2 + r_3 q_3 - r_1 q_0)$
C	$-\frac{k_b}{r_1^2} r_2 (r_2 q_2 + r_3 q_3 + r_1 q_0)$	$-\frac{k_b}{r_1^2} r_3 (r_2 q_2 + r_3 q_3 + r_1 q_0)$	$r_2 q_2 + r_3 q_3 + r_1 q_0 > 0$	$-\frac{k_b}{r_1^2} (r_2 q_2 + r_3 q_3 + r_1 q_0)$
D	$\frac{k_b}{r_1^2} r_2 (-r_2 q_2 - r_3 q_3 - r_1 q_0)$	$\frac{k_b}{r_1^2} r_3 (-r_2 q_2 - r_3 q_3 - r_1 q_0)$	$-r_2 q_2 - r_3 q_3 - r_1 q_0 > 0$	$-\frac{k_b}{r_1^2} (-r_2 q_2 - r_3 q_3 - r_1 q_0)$

where τ_b is the torque produced by the BPEA between joints 2 and 3, and is given by Table II. Naturally, it is possible to combine PEAs and BPEA. In this case, (5) becomes:

$$M(q)\ddot{q} + C(q,\dot{q})\dot{q} + G(q) = \tau_l + \tau_p + \tau_b \tag{6}$$

C. Actuator Electrical Energy Consumption

We first explain the relation between (1) and the electrical energy consumption of the robotic arm actuators. A robot with 3 electrical servo actuators with harmonic drive transmission can be modelled as follows (when the effects of the inductance are neglected):

$$J_{m,i}\ddot{q}_i + \nu_i \dot{q}_i = k_{t,i} I_i - \tau_{f,i}(\dot{q}_i, \tau_{l,i}) \tag{7}$$

$$U_i = R_i I_i + k_{t,i}\dot{q}_i \tag{8}$$

where $J_{m,i}$ are the inertia of the actuators, ν_i are the actuators' friction coefficient, $k_{t,i}$ are the actuators' torque constant, I_i are the actuators' current, $\tau_{f,i}(\dot{q}_i, \tau_{l,i})$ are the torques due to the load and the losses in the harmonic drive, U_i are the actuators' voltage, R_i are the electrical winding resistance of the actuators, and $i = 1, 2, 3$ represent respectively joints 1, 2, and 3. Note that $\tau_{f,i}(\dot{q}_i, \tau_{l,i})$ depends linearly and increases monotonically with the load torque as observed experimentally with harmonic drives as transmissions. The electrical energy consumption of the actuators is given by the integral over the time of the product between the actuator current and voltage. By isolating the actuator current I_i in (7), and by taking into account that a pick-and-place task is considered, meaning that the term that includes the inertia is null, one obtains:

$$E = \sum_{i=1}^{3} \int_{t_0}^{t_f} U_i I_i = \sum_{i=1}^{3} \int_{t_0}^{t_f} (R_i I_i^2 + \nu_i \dot{q}_i^2 + \tau_{f,i}(\dot{q}_i, \tau_{l,i})\dot{q}_i) dt \tag{9}$$

One can see that there are mainly two ways to reduce the electrical energy consumption of electrical actuators when the task the robot has to fulfil can not be modified and that the trajectory is fixed (q is fixed): 1) An appropriate choice of the actuators, and 2) Use of energy buffers, like elastic elements, in order to reduce the load torques and therefore the torque requirements of the actuators. Since the second solution does not depend on the type of actuator used, the second solution is more general and is the one adopted in this letter. Indeed, by implementing elastic elements in the system, it is possible to reduce the first and third terms of (9) by storing and releasing gravitational energy, and therefore, the electrical energy consumption. In other words, by implementing parallel or biarticular springs, one can reduce the first and third terms of (9) by decreasing the load torque squared. Regarding the second term of (9), it does not depend on the optimization since the trajectory of the joints is fixed. Therefore, it is not necessary to include it in the cost function.

Furthermore, by looking at (7), one can see that the first term in (9) depends on the load torque squared. For this reason, in addition to all the reasons above, the cost function chosen for the simulation is:

$$E_l = \sum_{i=2}^{3} \int_{t_0}^{t_f} \tau_{l,i}^2(t) dt \tag{10}$$

Note that this cost function allows reducing at the same time the RMS and peak load torque while having a cost function which is always positive, leading to simpler numerical optimization computations. It is also important to mention that only the last two actuators are considered in the cost function because, as stated in Section II-B, joint 1 is not studied. Furthermore, both static and dynamic effects of the robot are taken into account in this cost function since $tau_{l,i}$ includes the gravitational torque, and the torques due to inertia, Coriolis, and centrifugal forces of the robot. Nevertheless, it is the gravitational torque that has the most influence on the load torque in our case.

D. Optimization Procedure

The goal is to find the optimal spring parameters (parallel and biarticular) minimizing (10). The optimization problem can be stated as:

$$\begin{aligned} &\underset{u}{\text{minimize}} \quad E_l \\ &\text{subject to} \quad h(x,u,t) = 0 \\ &\qquad\qquad c_{\min} \leq c(x,u,t) \leq c_{\max} \end{aligned} \tag{11}$$

Equation (11) is a NonLinear Programming (NLP) problem with x the state variables, u the unknowns of the problem being the elastic element properties (stiffness, equilibrium angles, pulley radii), $h(x,t) = 0$ equality constraints such as (6), and $c_{\min} \leq c(x,t) \leq c_{\max}$ inequality constraints such as maximum equilibrium angles and minimum/maximum stiffness for the elastic elements.

To perform the simulations and solve this NLP problem, the problem is implemented in AMPL [24] and solved using the non-linear programming solver Knitro [25]. As E_l is an integral, it is required to discretize it. There are several methods to do it, such as using Euler or Pseudo-Spectral (interpolation that uses the Chebyshev grid) methods. Only Pseudo-Spectral methods with polynomials have been used because they are simpler to

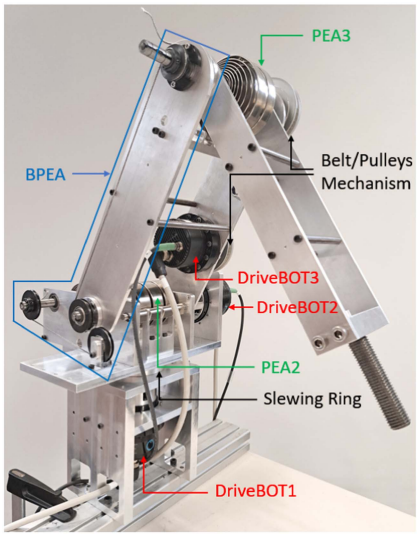

Fig. 7. Prototype. The terms written in red represent the actuators, those in green are the parallel springs, and the ones in black are the transmission mechanisms. The region surrounded in blue represent the BPEA with an Arrangement D.

implement compared to Pseudo-Spectral methods with trigonometric functions, and this without impacting significantly the results.

IV. Prototype

Based on the simulation results shown in Section V, a prototype has been built (Fig. 7). The 3 electrical servo actuators used are DriveBOT from the company Spinbotics with integrated brake. It has been designed to have the possibility to add PEAs on joints 2 and 3, and a BPEA between joints 2 and 3 with any arrangement thanks to a pulley mechanism. The third joint is actuated by a DriveBOT connected to a belt and pulleys mechanism with a pulley ratio of 1:1 with the aim of moving the mass of this DriveBOT closer to the base and therefore decreasing the torque requirements of the DriveBOT that actuates the second joint.

Note that the equilibrium angles of the PEAs and BPEA are set manually, which reduces the precision of their real implementation on the prototype by $\pm 5°$. The reason behind that is we did not want to implement additional motors to change them. Indeed, it will increase the weight and the electrical energy consumption of the robot for compensating only an error of maximum 5°. Moreover, based on the simulations' results, an error of 5° in the equilibrium angles of the PEAs or BPEA leads to an increase of less than 2% in terms of RMS load torques for both joints when compared to the simulations with optimal equilibrium angles. Therefore, this demonstrates the very small influence of this error on the efficiency of the PEAs and BPEA.

V. Simulation and Experimental Results

Three different optimizations and experiments have been performed. In the first, only PEAs are placed on joints 2 and 3. In the second, there is only a BPEA between joints 2 and 3, while in the last one, PEAs on joints 2 and 3 are placed simultaneously with a BPEA between joints 2 and 3. The task to fulfil is described in Section II-B, i.e. a pick-and-place task whereby a load of 5 kg is manipulated. The values of the optimal parameters of both optimizations are given in Table III.

TABLE III
Parallel Elastic Actuation and Biarticular Parallel Elastic Actuation Optimal Parameters

(a) PEA parameters

$k_{p,2}$	$13.7 Nm/rad$
$q_{eq,2}$	110°
$k_{p,3}$	$1.32 Nm/rad$
$q_{eq,3}$	140°

(b) BPEA parameters

k_b	$3.425 Nm/rad$
q_0	−150°
r_1	$19 mm$
r_2	$19 mm$
r_3	$14 mm$

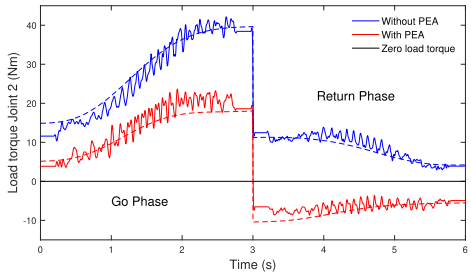

(a) Joint 2

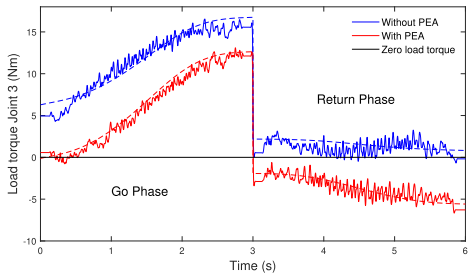

(b) Joint 3

Fig. 8. Influence of the optimal PEAs on the load torque for joints 2 and 3. Dashed lines indicate simulation results while solid lines are for experimental results.

A. Optimal Configuration of Parallel Elastic Actuations

As mentioned in Section III-A, both orientations of the parallel springs have been examined. Nevertheless, since the gravitational torque is the dominant term in (1) and is always oriented in the same direction, only the case where the torque produced by the parallel spring is countering the gravitational torque can be energy-efficient. The results obtained for the load torque in this case for joints 2 and 3 are shown in Fig. 8. One can see that implementing such PEAs on joints 2 and 3 can reduce the influence of the gravitational torques on the load torques for both joints. Reductions in RMS and peak load torques are given in Table IV. Furthermore, one can see that for both joints, the load torque with PEA is above zero for the go phase and below zero for the return phase. This can be explained by the

TABLE IV
REDUCTIONS IN RMS AND PEAK LOAD TORQUES FOR SIMULATIONS AND EXPERIMENTS

		PEAs		BPEA		PEAs and BPEA	
		RMS	Peak	RMS	Peak	RMS	Peak
Joint 2	Simulations	8.5Nm (44%)	21.6Nm (55%)	6.9Nm (36%)	9.5Nm (24%)	8.5Nm (44%)	21.6Nm (55%)
	Experiments	8.3Nm (43%)	18.5Nm (44%)	6.3Nm (33%)	7.8Nm (19%)	7.9Nm (41%)	19.5Nm (49%)
Joint 3	Simulations	1Nm (15%)	4.1Nm (25%)	1Nm (15%)	7Nm (42%)	1.2Nm (18%)	7.5Nm (45%)
	Experiments	1Nm (15%)	3.4Nm (21%)	0.8Nm (12%)	6.7Nm (40%)	1.1Nm (16%)	7.2Nm (43%)

The absolute and relative decreases are given with respect to the case without any springs.

fact that parallel springs provide a torque that decreases the load torque, and which is the same for the return and go phase but mirrored. However, since the load torque without PEA is higher in the go phase than in the return phase, the load torque with PEA is above zero for the go phase and drops below zero for the return phase due to the parallel springs. This phenomenon appears because the cost function is the squared load torque, meaning that the sign of the load torque has no importance in the optimization. This explains that for joint 2, the load torque is almost the same but of opposite sign for the return phase for the cases with and without PEA. Note that with this configuration, the electrical energy consumption has been reduced by 44% and 5% respectively for joints 2 and 3.

B. Optimal Configuration of Biarticular Parallel Elastic Actuation

As mentioned in Section III-B, there are four different possibilities for the arrangements of a BPEA. Therefore, four arrangements have been examined and compared together to see which one can result in the largest decrease in electrical energy consumption. Out of the four arrangements and based on the equations given in Table II, only Arrangement D produces a torque on joints 2 and 3 that counteracts the effect of gravity, so it is expected that this is the optimal arrangement. This has been confirmed by simulations and experiments. One can observe the influence of the biarticular spring on the load torque of joints 2 and 3 in Fig. 9. As for PEA, BPEA mainly decreases the influence of the gravitational torque on the load torque for both joints. The decreases in RMS and peak load torques are displayed in Table IV, and one can conclude that implementing PEAs is more energy-efficient than implementing BPEA.

C. Optimal Configuration of Combined Parallel Elastic Actuations and Biarticular Parallel Elastic Actuation

After having optimized the PEAs and BPEA separately, it is also interesting to investigate whether it is possible to reach higher RMS and peak load torques decrease by optimizing both concurrently. The results obtained are shown in Table IV. One can see that there is only a minor improvement compared to the reduction obtained by PEAs alone. As a result, PEAs on joints 2 and 3 is the best compromise in terms of energy efficiency and system complexity.

D. Influence of the Payload Release

PEAs have been optimized on joints 2 and 3 for the entire task, namely the go and return phases together. Looking at Fig. 6, one

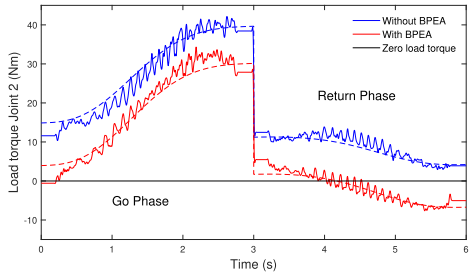

(a) Joint 2

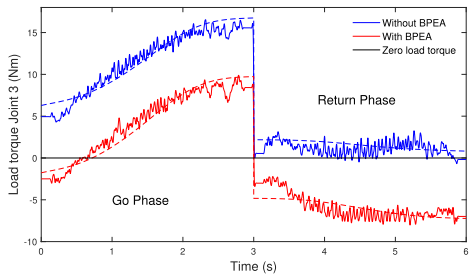

(b) Joint 3

Fig. 9. Influence of the optimal BPEA on the load torque for Joints 2 and 3. Dashed lines indicate simulation results while solid lines are for experimental results.

TABLE V
REDUCTIONS IN RMS AND PEAK LOAD TORQUES FOR PARALLEL ELASTIC ACTUATIONS OPTIMIZED PER PHASE

	Joint 2		Joint 3	
	RMS	Peak	RMS	Peak
Go	28.9Nm (97%)	38Nm (96%)	6.8Nm (55%)	8.6Nm (51%)
Return	8.2Nm (96%)	10.8Nm (95%)	0.9Nm (55%)	1.1Nm (51%)
Both	18.6Nm (96%)	38Nm (96%)	3.9Nm (55%)	8.6Nm (51%)

The absolute and relative decreases are given with respect to the case without any springs.

can see that, with the optimal configuration of PEAs, for both joints, the decrease in both RMS and load torque is much higher for the go phase than for the return phase. Furthermore, the optimal PEA on joint 3 increases the RMS and peak load torque in the return phase as shown in Fig. 6(b).

Suppose now that the PEAs are optimized for each phase individually, which is very similar to having no payload release. In this case, one can see in Table V that it is possible to reach a high decrease in RMS and peak load torque on both joints. Therefore, the optimization of PEAs for a pick-and-place task consists in reality of the optimization of two competing objectives. Indeed, it consists of the optimization of each phase, where the optimization results are a trade-off depending on the

relative duration of one phase compared to the other (as both phases are symmetric). If the go phase lasts longer than the return phase, the optimization of the pick-and-place will be more similar to the optimization of the go phase only than the return phase only, and inversely.

Therefore, one can conclude that the payload release has a negative impact on the RMS and peak load torque reductions. Moreover, one can also observe that the more the variation of the payload between both phases is high, the less the relative decrease in RMS load torque can be large. Finally, minimizing the duration of one phase over the other is beneficial for the efficiency of PEAs. In the case of pick-and-place tasks, it is better to minimize the duration of the return phase, namely where the load torques are lower.

VI. Conclusion

In this letter, an optimal configuration of PEA and BPEA, and optimal springs' characteristics for a given pick-and-place task performed by a 3 degrees of freedom robotic arm have been studied. It has been shown that the optimal configuration for this specific task in terms of electrical energy consumption and system complexity consists of a rigid actuation on joint 1 and PEAs on joints 2 and 3. Such a configuration can decrease the RMS and peak load torques respectively by 43% and 44% on joint 2, and by 15% and 21% on joint 3. Nevertheless, both PEA and BPEA can help to decrease the RMS and peak load torque mainly due to gravity when they are optimized for a specific task, but they show limitations due to the payload release. However, this conclusion is based on several limitations: 1) Specific task (task time and payload), 2) Fixed trajectory, 3) Type of control, 4) Limited choices of the radii of the BPEA pulleys, and 5) Constant radii of the BPEA pulleys. Future work will consist of extending the simulations and experiments to different task times, payloads, trajectories, types of control, and other mechanisms than SEA, PEA, and BPEA. Another strategy would be to use co-optimization, namely the optimization of the mechanical design and the control simultaneously.

References

[1] J. James, P. Ross, and D. Ball, "Comparison of elastic configurations for energy efficient legged locomotion," in *Proc. IEEE Int. Conf. Robot. Automat.*, 2015, pp. 1–7.

[2] G. Pratt and M. Williamson, "Series elastic actuators," in *Proc. IEEE/RSJ Int. Conf. Intell. Robots Syst. Hum. Robot Interact. Cooperative Robots*, 1995, pp. 399–406.

[3] S. Wang, W. van Dijk, and H. van der Kooij, "Spring uses in exoskeleton actuation design," in *Proc. IEEE Int. Conf. Rehabil. Robot.*, 2011, pp. 1–6.

[4] T. Verstraten, P. Beckerle, R. Furnémont, G. Mathijssen, B. Vanderborght, and D. Lefeber, "Series and parallel elastic actuation: Impact of natural dynamics on power and energy consumption," *Mechanism Mach. Theory*, vol. 102, pp. 232–246, Aug. 2016.

[5] Y. Yesilevskiy, W. Xi, and C. D. Remy, "A comparison of series and parallel elasticity in a monoped hopper," in *Proc. IEEE Int. Conf. Robot. Automat.*, 2015, pp. 1036–1041.

[6] M. Grimmer, M. Eslamy, and A. Seyfarth, "Energetic and peak power advantages of series elastic actuators in an actuated prosthetic leg for walking and running," *Actuators*, vol. 3, pp. 1–19, Feb. 2014.

[7] D. F. B. Haeufle, M. D. Taylor, S. Schmitt, and H. Geyer, "A clutched parallel elastic actuator concept: Towards energy efficient powered legs in prosthetics and robotics," in *Proc. IEEE 4th RAS EMBS Int. Conf. Biomed. Robot. Biomechatronics*, 2012, pp. 1614–1619.

[8] P. Beckerle, T. Verstraten, G. Mathijssen, R. Furnemont, B. Vanderborght, and D. Lefeber, "Series and parallel elastic actuation: Influence of operating positions on design and control," *IEEE/ASME Trans. Mechatronics*, vol. 22, no. 1, pp. 521–529, Feb. 2017.

[9] F. Gao, W.-H. Liao, B. Chen, H. Ma, and L.-Y. Qin, "Design of powered ankle-foot prosthesis driven by parallel elastic actuator," in *Proc. IEEE Int. Conf. Rehabil. Robot.*, 2015, pp. 374–379.

[10] M. Plooij and M. Wisse, "A novel spring mechanism to reduce energy consumption of robotic arms," in *Proc. IEEE/RSJ Int. Conf. Intell. Robots Syst.*, 2012, pp. 2901–2908.

[11] J. Babič, B. Lim, D. Omrčen, J. Lenarčič, and F. C. Park, "A biarticulated robotic leg for jumping movements: Theory and experiments," *J. Mechanisms Robot.*, vol. 1, Feb. 2009, Art. no. 011013.

[12] M. M. Pelit, J. Chang, and M. Yamakita, "Effects of passive biarticular muscles on walking performance for bipedal robots," in *Proc. IEEE/ASME Int. Conf. Adv. Intell. Mechatronics*, 2021, pp. 917–922.

[13] G. J. V. I. Schenau, "From rotation to translation: Constraints on multi-joint movements and the unique action of bi-articular muscles," *Hum. Movement Sci.*, vol. 8, pp. 301–337, Aug. 1989.

[14] B. Lim, J. Babic, and F. Park, "Optimal jumps for biarticular legged robots," in *Proc. IEEE Int. Conf. Robot. Automat.*, 2008, pp. 226–231.

[15] D. Lahr and H. Yi, "Improving the energy efficiency of bipedal robots with bi-articular actuation," *J. Adv. Mech. Des. Syst., Manuf.*, vol. 11, no. 5, 2017, Art. no. JAMDSM0058.

[16] V. Salvucci, Y. Kimura, S. Oh, T. Koseki, and Y. Hori, "Comparing approaches for actuator redundancy resolution in biarticularly-actuated robot arms," *IEEE/ASME Trans. Mechatronics*, vol. 19, no. 2, pp. 765–776, Apr. 2014.

[17] S. Oh, V. Salvucci, Y. Kimura, and Y. Hori, "Mathematical and experimental verification of efficient force transmission by biarticular muscle actuator," *IFAC Proc. Volumes*, vol. 44, pp. 13516–13521, Jan. 2011.

[18] H. Choi, S. Oh, and K. Kong, "Design of a biarticular robotic manipulator and its control in the rotating coordinate system," in *Proc. IEEE/ASME Int. Conf. Adv. Intell. Mechatronics*, 2014, pp. 888–891.

[19] H. J. Bidgoly, A. Parsa, M. J. Yazdanpanah, and M. N. Ahmadabadi, "Benefiting from kinematic redundancy alongside mono- and biarticular parallel compliances for energy efficiency in cyclic tasks," *IEEE Trans. Robot.*, vol. 33, no. 5, pp. 1088–1102, Oct. 2017.

[20] C. Chevallereau, P. Wenger, Y. Aoustin, F. Mercier, N. Delanoue, and P. Lucidarme, "Leg design for biped locomotion with mono-articular and bi-articular linear actuation," *Mechanism Mach. Theory*, vol. 156, Feb. 2021, Art. no. 104138.

[21] N. M. Cahill, T. Sugar, Y. Ren, and K. Schroeder, "Optimal stiffness design for an exhaustive parallel compliance matrix in multiactuator robotic limbs," *J. Mechanisms Robot.*, vol. 10, Jun. 2018, Art. no. 031014.

[22] T. Morizono, K. Tahara, and H. Kino, "A study on effect of biarticular muscles in an antagonistically actuated robot arm through numerical simulations," *Artif. Life Robot.*, vol. 22, pp. 74–82, Mar. 2017.

[23] U. Mettin, P. X. La Hera, L. B. Freidovich, and A. S. Shiriaev, "Parallel elastic actuators as a control tool for preplanned trajectories of underactuated mechanical systems," *Int. J. Robot. Res.*, vol. 29, pp. 1186–1198, Aug. 2010.

[24] R. Fourer, D. M. Gay, and B. W. Kernighan, "AMPL: A mathematical programming language," in *Algorithms and Model Formulations in Mathematical Programming*. Berlin, Germany: Springer, 1989, pp. 150–151.

[25] R. H. Byrd, J. Nocedal, and R. A. Waltz, "KNITRO: An integrated package for nonlinear optimization," in *Large-Scale Nonlinear Optimization* (Series Title: Nonconvex Optimization and Its Applications), vol. 83, P. Pardalos, G. Di Pillo, and M. Roma, eds. Boston, MA, USA: Springer, 2006, pp. 35–59.